nature communications

Article

https://doi.org/10.1038/s41467-025-64709-z

Streamlined construction of boron-stereogenic BODIPY library for near-infrared bioimaging

Received: 8 April 2025

Accepted: 25 September 2025

Jiayi Zhao[1,4], **Li-Qing Ren**[1,4], **Deren Lan**[2,4], **Baoquan Zhan**[1], **Jinyuan Zhang**[2], **Jing Mu**[3] & **Chuan He**[1]

Chirality is fundamental to molecular recognition, critically influencing pharmaceutical interactions, biomolecular sensing, and chiroptical device performance. While chiroptical luminophores hold transformative potential for optoelectronic innovation and precision bioimaging, their rational engineering remains constrained by synthetic limitations. Here, we report a streamlined and programmable asymmetric synthesis platform enabling systematic construction of boron-stereogenic boron dipyrromethene (BODIPYs) with near-infrared (NIR) chiroptical activity. This approach enables precise functionalization of prochiral BODIPYs via catalytic enantioselective cross-coupling, affording increased π-conjugated dyes with excellent enantiomeric excess and tunable photophysical properties. Further study demonstrates that molecular chirality plays a critical role in cellular recognition, as our chiral BODIPY dyes exhibit enantioselective uptake and distinct subcellular localization in cells. When formulated as nanoparticles, these dyes enable high-resolution NIR-II vascular imaging. This work not only establishes boron-centered stereogenicity as a design paradigm for advanced chiroptical bioimaging probes but also unveils dimensions in chiral organoboron chemistry with implications spanning from targeted therapeutics to chiral photonics.

Chirality plays a pivotal role in medicinal chemistry, as different enantiomers of a drug often exhibit significantly distinct therapeutic effects, toxicity profiles, side effects, and pharmacokinetics[1–4]. As a result, regulatory agencies mandate the evaluation of the bioactivity of all stereoisomers of pharmaceutical candidates during the drug discovery and development process, given the chiral nature of enzymes and receptors in biological systems (Fig. 1a, left). Similarly, chirality plays a crucial role in the development of fluorescent probes[5–7]. Chiral structures can enhance probe specificity by stereochemically matching target proteins, provide deeper insights into molecular chiral interactions, and enable the identification of biomarkers for disease diagnosis with improved detection sensitivity (Fig. 1a, right). However, despite notable progress in chiroptical fluorescent probes in recent decades, the creation of a library of such probes with well-defined structure-function relationships, particularly for applications in cellular recognition and biological imaging, remains an unmet challenge.

On the other hand, near-infrared (NIR) absorbing/emitting dyes have garnered significant attention due to their broad applications across fields such as photovoltaic cells, biology, and optoelectronics[8–13]. Operating in the red/NIR region offers distinct advantages, primarily because of the "biological window" spanning the range of 650–1000 nm. This spectral range minimizes issues such as autofluorescence, water absorption, tissue absorption, and cellular interference, while also reducing light scattering[14–17] (Fig. 1b). Therefore, the development of

---

[1]Shenzhen Grubbs Institute and Department of Chemistry, Shenzhen Key Laboratory of Small Molecule Drug Discovery and Synthesis, Guangdong Provincial Key Laboratory of Catalysis, Southern University of Science and Technology, Shenzhen, Guangdong, China. [2]Department of Nuclear Medicine, Peking University Shenzhen Hospital, Shenzhen, China. [3]Institute of Precision Medicine, Peking University Shenzhen Hospital, Shenzhen, China. [4]These authors contributed equally: Jiayi Zhao, Li-Qing Ren, Deren Lan. e-mail: jing.mu@pkuszh.com; hec@sustech.edu.cn

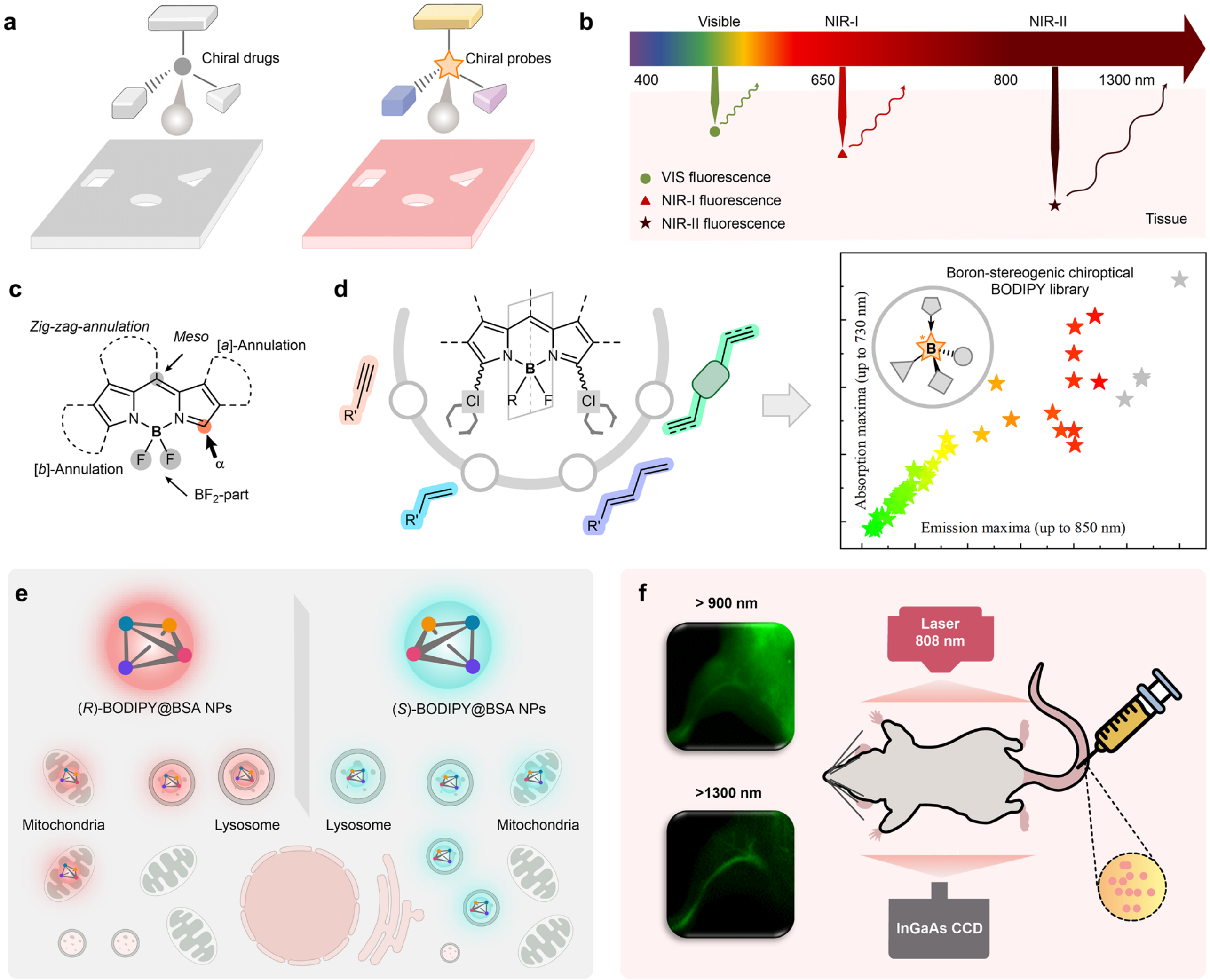

Fig. 1 | Design for red/NIR boron-stereogenic BODIPY dyes. **a** The critical role of chirality in the molecular recognition of drugs and fluorescent probes. **b** Advantages and broad applications of NIR-absorbing/emitting dyes. **c** Strategies for tuning BODIPY absorption into the far-red and NIR regions. **d** Streamlined construction of chiroptical NIR BODIPY library via palladium-catalyzed enantioselective cross-coupling reactions. **e** Chiral-dependent subcellular localization of BODIPY@BSA in U87 cells. **f** High-resolution NIR-II imaging of BODIPY@BSA for in vivo vascular visualization.

fluorescent materials within this region is highly attractive and in demand. Among various NIR chromophores[18,19], the boron dipyrromethene (BODIPY) dye family stands out as one of the most reliable NIR fluorophores. Due to their exceptional properties, including high molar absorption coefficients, high fluorescence quantum yields, sharp absorption and emission peaks, excellent biocompatibility, and photostability, BODIPY dyes have found extensive applications in bioimaging, photodynamic therapy, and optoelectronic materials[20–23]. However, conventional BODIPY dyes typically exhibit absorption/emission maxima in the range of 470– 530 nm. To extend their utility into the far-red and NIR regions, several strategies have been employed (Fig. 1c): a) incorporating π-conjugated systems at the α-position; b) modifying the meso position; c) altering the boron center by replacing fluorine with other substituents; d) extending the π-conjugation through peripheral annulation[24–27]. Among these approaches, the most widely adopted involves expanding the conjugated system with aromatic alkynyl/alkenyl groups at the α-position. This method results in significant red-shifts in absorption and emission, making the modified BODIPY dyes highly suitable for applications in bioimaging, biophotonics, and information encryption[28–31].

Building on our group's longstanding interest in boron-stereogenic compounds[32–36], we sought to merge boron-stereogenic centers[37–40] with red/NIR α-alkynyl/alkenyl substituted BODIPY emitters, aiming to build a streamlined library of chiroptical red/NIR boron-stereogenic BODIPYs. While several chiroptical BODIPY dyes have been designed for red/NIR luminophores, efficient catalytic enantioselective synthetic methods for the programmed synthesis of boron-stereogenic BODIPYs remain elusive[41,42]. In light of this, we hypothesized that using prochiral dichloro BODIPYs as starting materials and employing enantioselective cross-coupling reactions with alkynes and alkenes could enable the synthesis of α-alkynyl/alkenyl substituted boron-stereogenic red/NIR BODIPYs. This approach would establish a platform for creating a chiroptical NIR boron-stereogenic BODIPY library and facilitate the exploration of the biological interactions of these chiral probes.

Herein, we report the streamlined construction of boron-stereogenic BODIPYs with NIR chiroptical activity via palladium-catalyzed enantioselective Sonogashira and Heck reactions (Fig. 1d). Using phosphoramidite ligands with axial and central chirality, as well as bulky amine substituents, we synthesize a wide range of highly functionalized boron-stereogenic BODIPYs with α-alkynyl/alkenyl/dienyl substitutions, achieving good to excellent enantioselectivities. Notably, the α-chloro-substituted BODIPY products can undergo further post-functionalization to extend their conjugation, delivering structurally diverse chiral alkynyl/alkenyl/dienyl BODIPY derivatives. These chiral luminophores exhibit red-shifted absorption and emission profiles, demonstrating strong potential for bioimaging applications. By co-assembling with bovine serum albumin (BSA) to form BODIPY@BSA nanoparticles, they are subsequently applied in bioimaging studies. Uptake and subcellular localization experiments in U87 cells reveal a chiral-dependent distribution of BODIPY@BSA between lysosomes and mitochondria (Fig. 1e). Additionally, these nanoparticles demonstrate superior NIR-II imaging capabilities in in vivo vascular imaging, providing high-resolution with minimal background interference (Fig. 1f). The biocompatibility of BODIPY@BSA is further confirmed through biodistribution and histological analysis, establishing its potential as a promising NIR-II probe for real-time vascular monitoring.

Results and discussion

Establishment of boron-stereogenic BODIPY library

Based on our design, a prochiral BODIPY core **1a** with two α C-Cl bonds and phenylacetylene was selected as the starting material for condition screening. Reaction parameters, including ligands, bases, and solvents, were systematically optimized (Table S1). The optimal conditions were established using a phosphoramidite ligand bearing both axial and central chirality (**L**), CsOAc as the base, and *tert*-butyl methyl ether (TBME) as the solvent, resulting in a 96% yield and 99% ee for product **3a** after a 4-hour reaction. With the optimized conditions in hand, a variety of alkynyl-substituted BODIPYs with diverse photophysical properties were synthesized in high yield with excellent ee (Fig.2 left). For products with emission maxima in the 560–590 nm range, various substituted phenylacetylenes reacted efficiently. Alkynes bearing electron-withdrawing (Br, Cl, NO_2) or electron-donating (Me, acetyl) groups at the para-position of the aromatic ring produced the desired products **3a**-**3f** with good to excellent yields. Ortho-substituted aromatic alkynes (F, Cl, Br) afforded products **3g**-**3i** with similarly high yields and enantioselectivities, while meta-substituted aromatic alkynes (Cl, Br, OMe) were also well tolerated, delivering **3j**-**3l** with excellent results. Additionally, heteroaromatic alkynes, such as 3-ethynylthiophene, underwent a smooth reaction, yielding **3 m** with excellent yield and ee. Moreover, linear alkyl-substituted alkyne was also compatible, yielding product **3n** without any difficulty. For emission maxima below 560 nm, trimethylsilylacetylene was proven compatible with the reaction conditions, yielding the corresponding product **3o**, which could further be converted into terminal alkynes to expand structural diversity. To achieve red-shifted absorption and emission, aromatic alkynes with extended conjugation were explored. In the 590–610 nm range, 9-ethynyl-anthracene successfully produced product **3p** with a high fluorescence quantum yield. Similarly, tetraphenylethene (TPE)-functionalized alkyne **2q** was fully compatible, affording TPE-containing BODIPY derivative **3q**, which displayed red-shifted emission and potential aggregation-induced emission (AIE) activity[43]. Notably, alkynes with methoxy groups at the para or ortho position resulted in a significant red-shift (**3r**-**3s**) compared to other substituents (**3a**-**3l**). This is probably due to the electron-donating nature of the methoxy group, which facilitates intramolecular charge transfer. In light of this, alkynes with stronger electron-donating groups were tested to further red-shift the emission. As expected, para-substituted NPh_2 and NMe_2 groups produced products **3t** and **3 u** with emission maxima of 751 nm and 738 nm, respectively, both falling within the NIR region. Moreover, the scope was further expanded by modifying the dipyrromethene core and boron substituents using 4-ethynyl-*N*,*N*-dimethylaniline as the coupling partner. Replacing the phenyl group on the boron center with 3-thienyl led to product **3 v**, red-shifting the emission maximum by 12 nm. Additionally, substituting the meso group with electron-withdrawing groups improved the red shift. For example, pentafluorophenyl- and nitro-substituted derivatives (**3x** and **3w**) exhibited emission maxima of 774 nm and 798 nm, respectively, further extending the range into the NIR region.

Building on the successful synthesis of α-alkynyl boron-stereogenic BODIPYs via desymmetric Sonogashira coupling, we then aimed to expand our library by developing a rapid method for accessing α-alkenyl boron-stereogenic BODIPYs. After exploration, we discovered that replacing CsOAc with Et_3N as the base enabled the efficient synthesis of enantioenriched α-alkenyl boron-stereogenic BODIPYs via a Heck-type reaction between prochiral **1a** and alkenes **4** (Fig. 2 right). A broad range of alkenes with diverse functional groups and frameworks was evaluated, demonstrating the versatility of this method in producing structurally diverse α-alkenyl boron-stereogenic BODIPYs. For products with emission maxima in the 560-580 nm range, olefins containing functional groups such as acrylate (**4a**), acrylamide (**4b**), vinyl ether (**4c**), and vinyl silane (**4 d**), could be transformed into α-alkenyl boron-stereogenic BODIPYs (**5a**-**5d**) in excellent ee. Notably, vinylcyclohexane also participated in the reaction, affording the desired product with moderate yield and excellent ee. Aryl alkenes yielded products with pronounced red-shifted emission maxima. Substituents such as F, Cl, Br, ^{t}Bu, CF_3, and NO_2 at the ortho, meta, or para positions of the phenyl ring in alkenes delivered α-alkenyl boron-stereogenic BODIPYs (**5f**-**5m**) with good yields, excellent enantioselectivities, and emission maxima ranging from 580 to 599 nm. Similar to the alkynyl-substituted BODIPYs, para-OMe substitution on the phenyl ring significantly impacted the photophysical properties, with product **5o** showing an emission maximum at 611 nm. For products with emission maxima in the 600–620 nm range, substrates featuring extended conjugation, such as 9-phenylcarbazole (**4n**), 2-naphthyl (**4p**), and 2-thiophenyl (**4q**), were well tolerated, yielding the expected BODIPYs in high yields. Notably, 1-phenyl-1,3-butadiene (**4r**) also proceeded smoothly to afford **5r** with excellent yield and enantioselectivity. Product **5r** exhibited a 27 nm longer emission wavelength than **5 f**, likely due to the expanded π-conjugated system. Inspired by this result, we further investigated alkenes with fused aromatic rings (**4 s**) and other dienes (**4t**-**4v**) to construct NIR BODIPYs. The corresponding products **5s**-**5v** exhibited significant increases in both absorption and emission wavelengths. Product **5w** exhibited an emission maximum of 730 nm, attributed to the strong electron-donating property of 4-ethenyl-*N*,*N*-dimethylaniline. The photophysical data, including absorption maxima, emission maxima, and fluorescence quantum yields of each boron-stereogenic BODIPY, are listed in Fig. 2. In addition, the absorption and emission spectra of all products are provided in the Supplementary Information (Figs. S1–3).

Synthetic applications

To further red-shift the absorption and emission wavelengths of the obtained boron-stereogenic BODIPYs and demonstrate the downstream utility of this methodology, we conducted post-functionalization of α-chloro-substituted BODIPY products (Fig. 3a). First, a di-α-chloro-BODIPY, featuring different aryl groups on the meso-position, underwent efficient tandem alkynylation/alkenylation reactions, giving access to highly functionalized 3,5-disubstituted chiroptical BODIPY products **6a**-**6e** in decent total yields with excellent ee values and 750–850 nm emission wavelength. It is noteworthy that these structurally diverse enantioenriched alkynyl/alkenyl/dienyl BODIPY derivatives with different substitutions on both α-sites were previously inaccessible. Moreover, we successfully synthesized 1,4-bisalkynylbenzene/bisalkenylbenzene-bridged BODIPY dimers **6 f** and **6 g** in a smooth manner, with 99% ee and >20:1 *dr*. The unique scaffold of these dimers holds great potential for applications in fluorescence imaging[30]. In addition, we examined the copper-catalyzed click reaction between **6b**, which bears a trimethylsilyl group, and azides with the core structures of bioactive molecules, including D-glucopyranoside and vitamin E (Fig. 3b). Encouragingly, we obtained the corresponding boron-stereogenic BODIPY triazole products **6 h** and **6i** in good yields with excellent diastereoselectivities. This finding underscores the

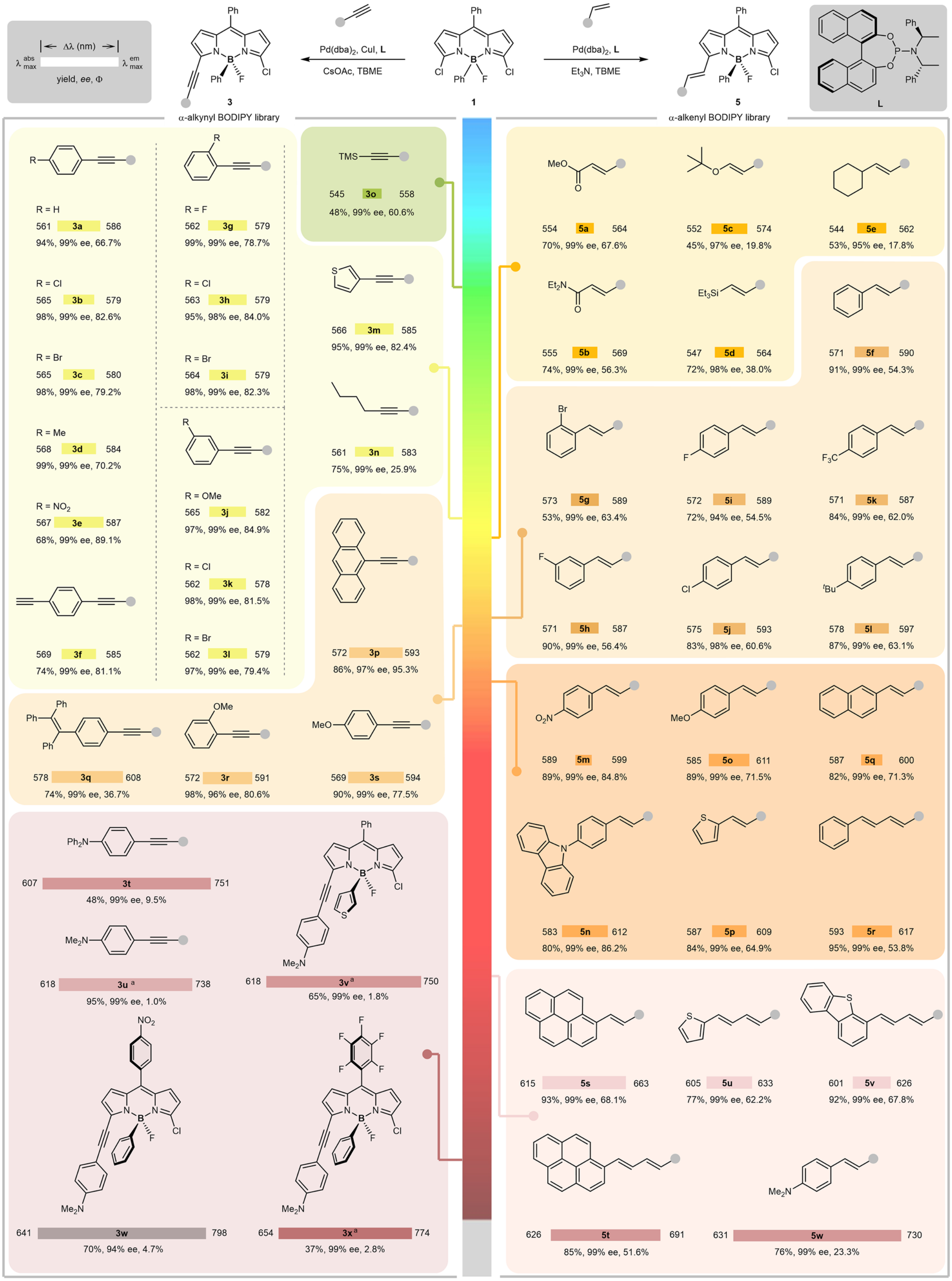

Fig. 2 | Establishment of boron-stereogenic BODIPY library. Reaction conditions of Sonogashira reaction: **1a** (0.1 mmol), **2** (0.1 mmol), Pd(dba)$_2$ (4 mol%), **L** (10 mol %), CsOAc (2.0 equiv) in 2.0 mL of TBME, under argon atmosphere, at 60 °C for 4 hours. Reaction conditions of Heck reactions **1a** (0.1 mmol), **4** (0.1 mmol), Pd(dba)$_2$ (4 mol%), **L** (10 mol%), Et$_3$N (2.0 equiv) in 2.0 mL of TBME, under argon atmosphere, at 80 °C for 10 hours. Photochemical properties are tested in CH_2Cl_2 (10^{-5} M), absorption maxima, emission maxima, and fluorescence quantum yields are listed below. The ee values were determined by chiral HPLC. [a]2.0 equiv of alkynes was used.

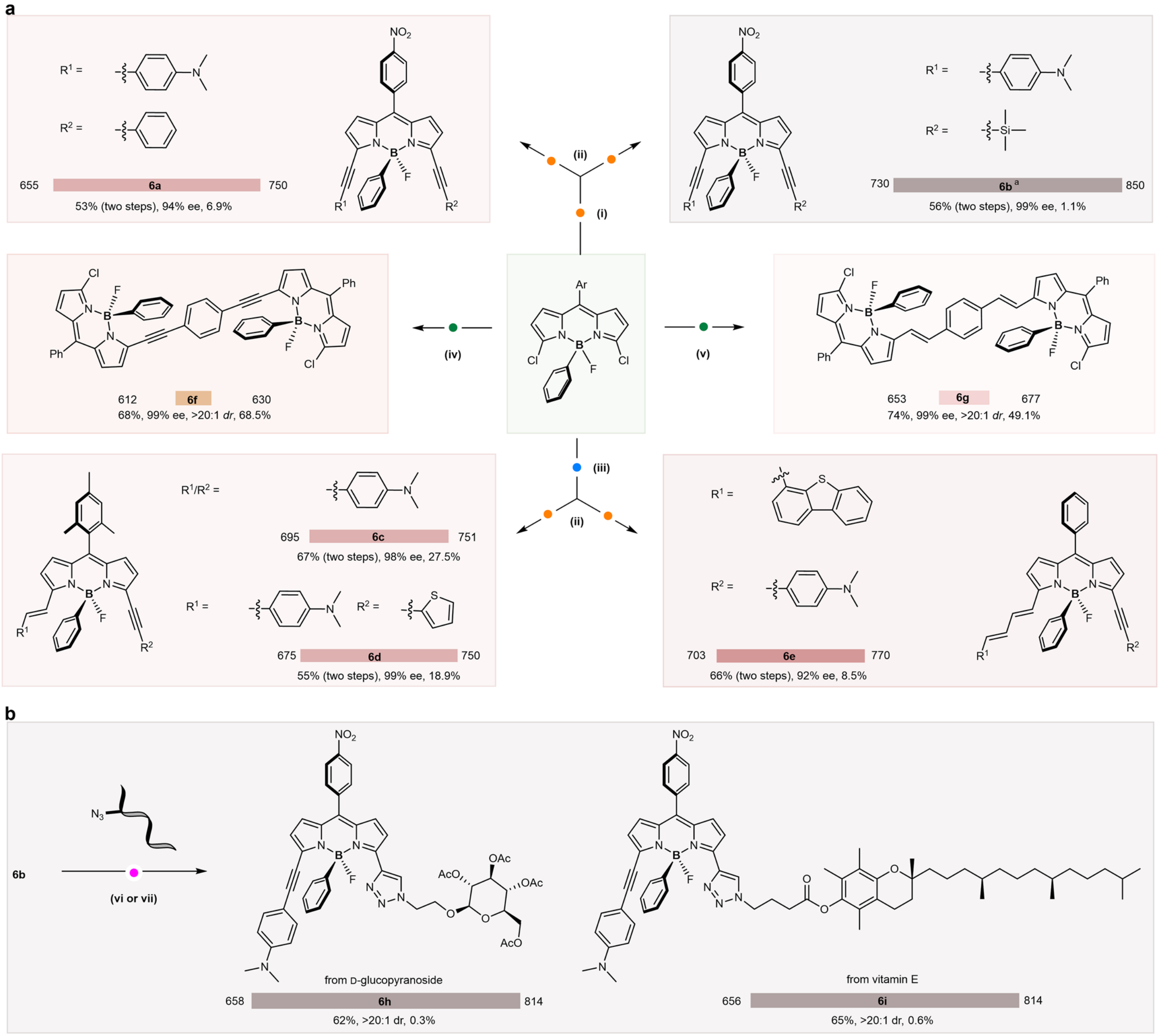

Fig. 3 | Synthetic applications. a Post-functionalization of boron-stereogenic 5-Cl-BODIPY. **b** Click reaction of α-alkynyl boron-stereogenic BODIPY. Reaction conditions: i) dichloro-BODIPY (0.1 mmol), alkyne (0.1 mmol), Pd(dba)$_2$ (4 mol%), CuI (5 mol%), **L** (10 mol%), CsOAc (2.0 equiv) in TBME at 60 °C for 4 hours. ii) α-chloro-BODIPY (0.05 mmol), alkyne (2.0 equiv), Pd(PPh$_3$)$_4$ (5 mol%), CuI (5 mol%), Et$_3$N (2.0 equiv) in THF at 80 °C for 12 hours. [a]CsOAc was used as the base, in TBME at 60 °C for 12 hours. iii) dichloro-BODIPY (0.1 mmol), alkene (0.1 mmol), Pd(dba)$_2$ (4 mol%), **L** (10 mol%), Et$_3$N (2.0 equiv) in TBME at 80 °C for 10 hours. iv) **1a** (0.1 mmol), 1,4-diethynylbenzene (0.05 mmol), Pd(dba)$_2$ (4 mol%), **L** (10 mol%), Et$_3$N (2.0 equiv) in toluene at 80 °C for 12 hours. v) **1a** (0.1 mmol), 1,4-diethenylbenzene (0.05 mmol), Pd(dba)$_2$ (4 mol%), **L** (10 mol%), Et$_3$N (2.0 equiv) in TBME at 80 °C for 12 hours. vi) **6b** (0.05 mol), azide (from **D**-glucopyranoside) (2.0 equiv), TBAF (1.0 equiv), Cu(MeCN)$_4$PF$_6$ (10 mol%) in DCM for 2 hours. vii) **6b** (0.05 mol), azide (from vitamin E) (2.0 equiv), AgBF$_4$ (20 mol%), Cu(MeCN)$_4$PF$_6$ (20 mol%) in DCM at 60 °C for 24 hours.

potential of the developed boron-stereogenic BODIPYs as promising chiral dyes for bioimaging and biofluorescent labeling applications.

Uptake and localization of BODIPY@BSA

Due to the inherent hydrophobicity of many BODIPY derivatives, direct use in aqueous biological systems can be challenging. To address this, we employed BODIPY@BSA complex in the following cellular and living studies. This formulation strategy provides several advantages, including enhanced water solubility, improved biocompatibility, and increased cellular uptake via BSA-mediated delivery. Details of the preparation and characterization are described in the Supplementary Information (Fig. S4). The biocompatibility of BODIPYs was also tested beforehand (Fig. S5 and 6), confirming that BODIPY@BSAs is safe enough for biomedical imaging.

The cellular uptake and intracellular localization of BODIPY@BSA were evaluated using confocal laser scanning microscopy. Human glioblastoma cell line U87MG cells were incubated with BODIPY@BSA for 2 hours, and strong red fluorescence was observed in the cytoplasm, indicating successful internalization of BODIPY@BSA (Fig. S7). To explore the impact of the chiral boron center on subcellular localization, colocalization studies were conducted using MitoTracker Green and LysoTracker Red. Live cell imaging (Fig. 4a, b) and corresponding colocalization analysis (Fig. 4c–f) revealed that *S*-**3w**@BSA exhibited high lysosomal specificity, as indicated by a Pearson correlation coefficient (PCC) of 0.896 with LysoTracker Red, significantly exceeding its mitochondrial colocalization (PCC = 0.492; $P \leq 0.0001$). In contrast, *R*-**3w**@BSA demonstrated comparable colocalization efficiency in both organelles (mitochondria: PCC = 0.53; lysosomes:

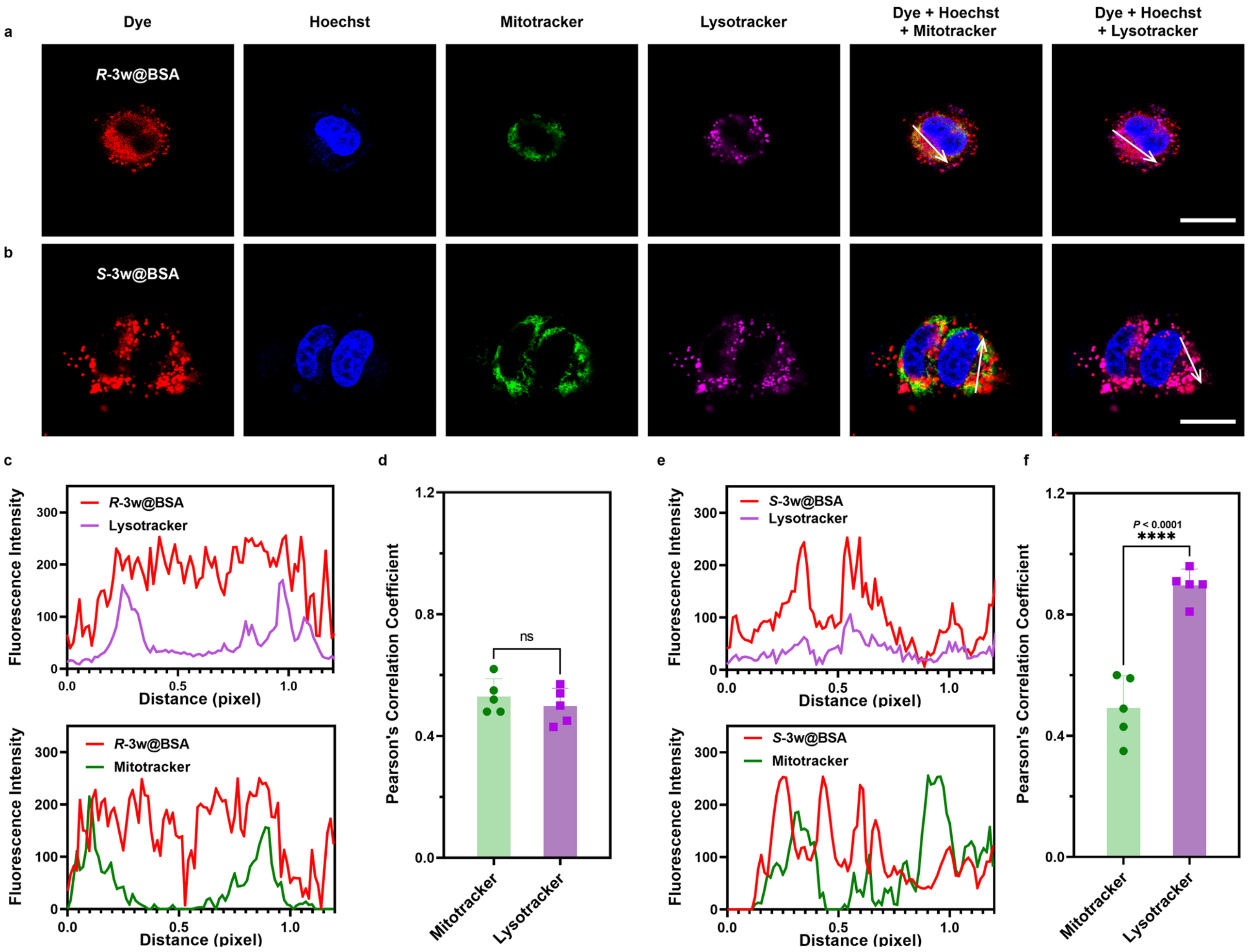

Fig. 4 | Live cell fluorescence imaging. a Fluorescence imaging of human glioblastoma cell U87MG costained with *R*-**3w**@BSA, MitoTracker Green and Lysotracker Red DND-99 (scale bar = 10 μm) ($n = 5$ independent experiments). **b** CLSM images of human glioblastoma cell U87MG costained with *S*-**3w**@BSA, MitoTracker Green and Lysotracker Red DND-99 (scale bar = 10 μm) ($n = 5$ independent experiments). **c** Fluorescence intensity plot of *R*-**3w**@BSA and Mitotracker or Lysotracker, respectively, in the corresponding merged figure ($n = 5$ independent experiments). **d** Histogram of Pearson correlation coefficients of *R*-**3w**@BSA with Mitotracker or Lysotracker ($n = 5$ independent experiments). **e** Fluorescence intensity plot of *S*-**3w**@BSA and Mitotracker or Lysotracker, respectively, in the corresponding merged figure ($n = 5$ independent experiments). **f** Histogram of Pearson correlation coefficients of *S*-**3w**@BSA with Mitotracker or Lysotracker ($n = 5$ independent experiments). Data are presented as mean ± SD. The assessment in (**d**, **f**) of *P* values was performed by a two-tailed Student's *t*-test; all tests were two-sided. ns: not significant (*P* value > 0.05); *****P* value < 0.0001. Source data are provided as a Source Data file.

PCC = 0.498; $P = 0.4131$). Additional colocalization experiments with other organelle markers showed negligible accumulation in the Golgi apparatus for both enantiomers (Fig. S8). Moderate overlap with lipid droplets was observed for **3w**@BSA, suggesting some lipophilic partitioning. Interestingly, both *R*-**3w**@BSA and *S*-**3w**@BSA showed moderate colocalization with the endoplasmic reticulum (ER), likely due to the physical contact and trafficking between ER and lysosomes.

To further elucidate the role of chirality in intracellular distribution, BSA was fluorescently labeled with FITC and used to encapsulate *R*- and *S*-**3w**, forming chiral BODIPY@BSA NPs. Fluorescence imaging showed partial spatial separation between BSA-FITC signals (green) and BODIPY signals (red), suggesting post-internalization dissociation of the dye from its protein carrier (Fig. S9). This observation implies that the differences in subcellular localization are primarily determined by the chirality of the BODIPY dye itself, rather than by the BSA vehicle. To further validate the generality of chiral-dependent organelle distribution, the intracellular distribution of other enantioenriched constructs **5w**@BSA and **6 g**@BSA was examined in U87MG cells. Consistent lysosomal enrichment was observed for both *S*-**5w** and (*S*,*S*)-**6g** (Fig. S10 and 11). Moreover, similar distribution patterns of **3w**@BSA were also observed in NIH/3T3 and Ocut-2C cells (Fig. S12 and 13). Collectively, these findings suggest that enantioselective interactions between BODIPY@BSA nanoparticles and chiral biomacromolecules, such as proteins, saccharides, and DNA, may contribute to the observed differences in subcellular localization.

NIR-II imaging with high resolution

In fluorescence imaging, spatial resolution is largely governed by the extent to which excitation and emission photons of the fluorophore can penetrate biological tissues[44]. To rigorously assess the imaging performance of BODIPYs within the NIR-II window, the clinically approved dye indocyanine green (ICG) served as a benchmark. As an initial step, Intralipid was employed as a tissue-mimicking phantom medium to visualize imaging behavior across varying penetration depths[45]. **6c** and **6e** were loaded into glass capillaries and subsequently submerged in Intralipid at distinct depths for evaluation. As illustrated in Fig. 5a, both **6c** and **6e** produced high-quality images of glass capillaries, whereas ICG exhibited a pronounced loss of visibility as depth increased. For the BODIPY-treated samples, the full width at half maximum (FWHM) of the capillary signal, an indicator of spatial resolution, remained stable across depths within the 3 mm thickness range (0.8–2.6), as shown in Fig. 5b. In contrast, ICG capillaries

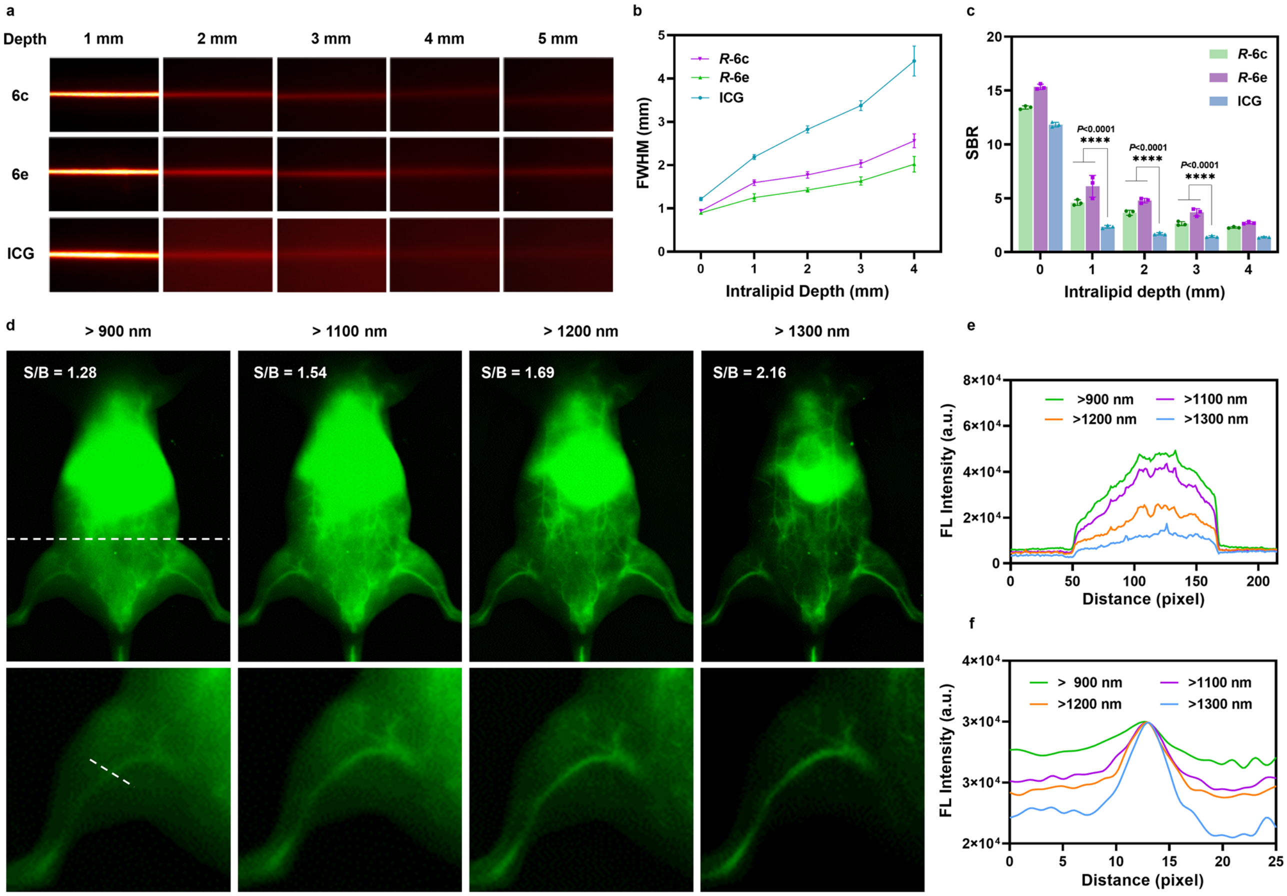

Fig. 5 | High-performance NIR-II fluorescence imaging. **a** NIR-II imaging of glass capillary tubes perfusing **6c, 6e**, and ICG solution, respectively, immersed in various depths of 1% intralipid solution ($n = 3$ independent experiments). **b** Correlation of FWHMs versus depths of intralipid solution ($n = 3$ independent experiments). **c** SBR calculation for the glass capillaries in A ($n = 3$ independent experiments). **d** NIR-II whole-body and femoral vessel imaging of **6c**@BSA ($n = 3$ mice). **e**, **f** Cross-sectional fluorescence signals profile of the NIR-II whole-body and femoral vessels imaging. Data are presented as mean ± SD. The assessment in (**c**) of *P* values was performed by a two-tailed Student's *t*-test; all tests were two-sided. ****P value < 0.0001. **e**, **f** a.u. indicates the arbitrary units. Source data are provided as a Source Data file.

exhibited a marked broadening of FWHM values, which diminished the signal-to-background ratio (SBR), a phenomenon likely linked to scattering effects in the NIR-II region. Furthermore, at all tested depths within the intralipid medium, BODIPYs consistently demonstrated superior SBRs relative to ICG (Fig. 5c). Collectively, these findings underscore the enhanced penetration depth and improved imaging contrast afforded by BODIPY dyes.

Blood vessels play a crucial role in nutrient transport and the maintenance of organ function. High-quality angiography is essential for efficient identification of vascular lesions and for evaluating postoperative blood flow recovery[46]. To assess the angiographic potential of BODIPYs, **6c**@BSA was intravenously injected into the tail vein of mice. Whole-body fluorescence angiography was performed under 808 nm laser excitation using various long-pass (LP) filters[47]. **6c**@BSA demonstrated superior NIR-II imaging capabilities for both systemic and local (leg) vasculature, as shown in Fig. 5d. Expanding the imaging window to longer wavelengths significantly improved image quality, particularly in the >1300 nm range, with minimal skin/background interference (S/B = 2.16). The cross-sectional fluorescence signal distribution in NIR-II whole-body and leg vascular imaging further demonstrated its capability to monitor vascular-related diseases (Fig. 5e, f).

The integration of molecular chirality into NIR fluorophores offers unique opportunities for enhancing imaging precision. In our study, boron-stereogenic BODIPY not only retains the excellent photophysical properties of traditional BODIPY dyes, such as high brightness, light stability, and tunable near-infrared emission, but also introduces chiral-driven recognition behaviors. To evaluate whether chirality affects in vivo imaging performance, we compared the biodistribution of *R*- and *S*-**3w**@BSA following intravenous injection into BALB/c mice. Ex vivo imaging of major organs at 6 hours post-injection (p.i.) revealed strong fluorescence signals in the gallbladder and intestine, indicating clearance via the hepatobiliary pathway. Interestingly, organ-specific signal intensity differed between enantiomers, with *S*-**3w**@BSA exhibiting higher accumulation in the liver and lower retention in the lung compared to *R*-**3w**@BSA (Fig. S14). These findings suggest that chirality may affect the in vivo biodistribution profiles. Additionally, the real-time NIR-II fluorescence imaging of **6c**@BSA and **6e**@BSA was also performed, and the biodistribution was quantified at 24 h p.i. (Fig. S15). Furthermore, H&E staining of major organs revealed no significant organ damage after 7 days post-injection, confirming favored in vivo biocompatibility (Fig. S16). These findings suggest that chiroptical BODIPYs may provide a promising tool for target-selective and high-resolution NIR imaging in living systems.

In summary, we have developed a streamlined catalytic asymmetric strategy, which powers boron-stereogenic BODIPYs for chiroptical near-infrared bioimaging. This efficient approach enabled the programmable functionalization of prochiral α-chloro BODIPYs, yielding highly conjugated boron-stereogenic dyes with excellent enantiomeric excess and red-shifted optical properties. These chiral luminophores not only exhibited enantioselective subcellular localization but also demonstrated superior NIR-II imaging capabilities for high-resolution vascular visualization. We believe that our results highlight the profound influence of chirality on molecular-level cellular recognition, offering valuable insights into the design of chiral fluorescent probes for precise bioimaging. By combining advanced optical properties with enantioselective behavior, these BODIPY dyes pave the way for next-generation diagnostic tools, enabling more accurate imaging of biological processes and the potential for real-time monitoring of disease progression.

Methods

General procedure towards α-alkenyl B-stereogenic BODIPYs

Inside an argon-filled glovebox, an oven-dried 5 mL microwave reaction tube was charged with $Pd(dba)_2$ (2.2 mg, 0.004 mmol), **L** (5.4 mg, 0.01 mmol), and TBME (1 mL). After stirring for 5 min, Et_3N (20.2 mg, 0.2 mmol), prochiral BODIPY **1a** (0.1 mmol, 39.6 mg), and **4** (0.1 mmol) were added, followed by the addition of TBME (1 mL). The tube was capped and removed from the glovebox. The resulting mixture was placed on a preheated (80 °C) aluminum block and stirred for 10 h. Then the reaction mixture was concentrated and purified by column chromatography to afford the target product.

General procedure towards α-alkynyl B-stereogenic BODIPYs

Inside an argon-filled glovebox, an oven-dried 5 mL microwave reaction tube was charged with $Pd(dba)_2$ (2.2 mg, 0.004 mmol), CuI (1.2 mg, 0.005 mmol), **L** (5.4 mg, 0.01 mmol), and TBME (1 mL). After stirring for 5 min, CsOAc (38.4 mg, 0.2 mmol), prochiral BODIPY **1a** (0.1 mmol, 39.6 mg), and alkyne (0.1 mmol) were added, followed by the addition of TBME (1 mL). The tube was capped and removed from the glovebox. The resulting mixture was placed on a preheated (60 °C) aluminum block and stirred for 4 h. The reaction mixture was concentrated and purified by column chromatography to afford the target product.

Cell lines and cell culture

Human glioblastoma cell U87MG and Mouse embryonic fibroblast cell NIH-3T3 were purchased from American Type Culture Collection (ATCC). Anaplastic thyroid carcinoma Ocut-2C was purchased from iCell Bioscience Inc. (Shanghai, China) (iCell-h389). All cell lines were cultured in DMEM mixed media with 10% (v/v) fetal bovine serum, 80 U/mL penicillin, and 0.08 mg/mL streptomycin in a relatively humidified atmosphere of 5% CO_2 at 37°C.

Animals

All animal experiments were conducted according to the protocols approved by the Research Ethics Committee of Shenzhen Peking University-The Hong Kong University of Science and Technology Medical Center (Procedure Number: 2022-938). Sex and/or gender were not considered in the study design, given that they were not hypothesized to influence the outcomes of this investigation. BALB/c nude mice (female, 6–8 weeks) were purchased from Gempharmatech Co., Ltd. Bedding, nesting material, food, and water were provided ad libitum. Ambient temperature was controlled at 24 °C to 26 °C in a humidity-controlled (60 ± 5%) environment with 12-hour light/12-hour dark cycles.

In vivo imaging

Female nude mice (6–8 weeks old) were injected with **6c**@BSA or **6e**@BSA via the tail vein and euthanized 24 hours later. Each mouse received 200 μL of solution at a concentration of 200 μg/mL. Upon excitation at 808 nm, signals were captured using a 900 nm long-pass filter. The biodistribution of **6c**@BSA and **6e**@BSA was assessed via NIR-II imaging in the heart, lungs, liver, spleen, and kidneys.

NIR-I biodistribution of 3w@BSA

Female nude mice (6–8 weeks old) were injected with *R*-**3w**@BSA or *S*-**3w**@BSA via the tail vein and euthanized 6 hours later. Each mouse was injected with 200 μL of a solution with a concentration of 200 μg/mL. The biodistribution of *R*-**3w**@BSA or *S*-**3w**@BSA in the heart, liver, spleen, lungs, stomach, kidneys, gallbladder, and intestines was evaluated by NIR imaging.

Reporting summary

Further information on research design is available in the Nature Portfolio Reporting Summary linked to this article.

Data availability

The data that support the findings of this study are available within the paper and its Supplementary Information files. Raw data are available from the corresponding author upon request. Materials and methods, experimental procedures, characterization data, ^1H, ^{13}C, ^{19}F, ^{11}B NMR spectra, and mass spectrometry data are available in the Supplementary Information. The X-ray crystallographic coordinates for structures reported in this study have been deposited at the Cambridge Crystallographic Data Center (CCDC), under deposition number CCDC 2361171 (**3l**). These data can be obtained free of charge from the CCDC via www.ccdc.cam.ac.uk/data_request/cif. Source data are provided with this paper.

References

1. Pfeiffer, C. C. Optical isomerism and pharmacological action, a generalization. *Science* **124**, 29–31 (1956).
2. Fabro, S., Smith, R. L. & Williams, R. T. Toxicity and teratogenicity of optical isomers of thalidomide. *Nature* **215**, 296–296 (1967).
3. Garay, A. S. Molecular chirality of life and intrinsic chirality of matter. *Nature* **271**, 186–186 (1978).
4. Milton, R. C. D., Milton, S. C. F. & Kent, S. B. H. Total chemical synthesis of a d-enzyme: The enantiomers of hiv-1 protease show reciprocal chiral substrate specificity. *Science* **256**, 1445–1448 (1992).
5. Pu, L. Fluorescence of organic molecules in chiral recognition. *Chem. Rev.* **104**, 1687–1716 (2004).
6. Zhang, X., Yin, J. & Yoon, J. Recent advances in development of chiral fluorescent and colorimetric sensors. *Chem. Rev.* **114**, 4918–4959 (2014).
7. Pu, L. Simultaneous determination of concentration and enantiomeric composition in fluorescent sensing. *Acc. Chem. Res.* **50**, 1032–1040 (2017).
8. Yuan, L., Lin, W., Zheng, K., He, L. & Huang, W. Far-red to near infrared analyte-responsive fluorescent probes based on organic fluorophore platforms for fluorescence imaging. *Chem. Soc. Rev.* **42**, 622–661 (2013).
9. Guo, Z., Park, S., Yoon, J. & Shin, I. Recent progress in the development of near-infrared fluorescent probes for bioimaging applications. *Chem. Soc. Rev.* **43**, 16–29 (2014).
10. Chen, Y., Yang, Y. & Zhang, F. Noninvasive in vivo microscopy of single neutrophils in the mouse brain via NIR-II fluorescent nanomaterials. *Nat. Protoc.* **19**, 2386–2407 (2024).
11. Yang, Y., Jiang, Q. & Zhang, F. Nanocrystals for deep-tissue in vivo luminescence imaging in the near-infrared region. *Chem. Rev.* **124**, 554–628 (2024).
12. Xu, C. & Pu, K. Second near-infrared photothermal materials for combinational nanotheranostics. *Chem. Soc. Rev.* **50**, 1111–1137 (2021).
13. Zhao, C. et al. Nanomedicines for an enhanced immunogenic cell death-based in situ cancer vaccination response. *Acc. Chem. Res.* **57**, 905–918 (2024).
14. Weissleder, R. A clearer vision for in vivo imaging. *Nat. Biotechnol.* **19**, 316–317 (2001).
15. Weissleder, R. & Pittet, M. J. Imaging in the era of molecular oncology. *Nature* **452**, 580–589 (2008).

16. Hong, G. et al. Through-skull fluorescence imaging of the brain in a new near-infrared window. *Nat. Photon.* **8**, 723–730 (2014).
17. Chen, S. et al. Near-infrared deep brain stimulation via upconversion nanoparticle–mediated optogenetics. *Science* **359**, 679–684 (2018).
18. Rao, R. S., Suman & Singh, S. P. Near-infrared (>1000 nm) light-harvesters: Design, synthesis and applications. *Chem. Eur. J.* **26**, 16582–16593 (2020).
19. Wang, Y., Yu, H., Zhang, Y., Jia, C. & Ji, M. Development and application of several fluorescent probes in near infrared region. *Dyes Pigm.* **190**, 109284 (2021).
20. Boens, N., Leen, V. & Dehaen, W. Fluorescent indicators based on BODIPY. *Chem. Soc. Rev.* **41**, 1130–1172 (2012).
21. Kamkaew, A. et al. BODIPY dyes in photodynamic therapy. *Chem. Soc. Rev.* **42**, 77–88 (2013).
22. Kowada, T., Maeda, H. & Kikuchi, K. BODIPY-based probes for the fluorescence imaging of biomolecules in living cells. *Chem. Soc. Rev.* **44**, 4953–4972 (2015).
23. Wang, J., Yu, C., Hao, E. & Jiao, L. Conformationally restricted and ring-fused aza-BODIPYs as promising near infrared absorbing and emitting dyes. *Coord. Chem. Rev.* **470**, 214709 (2022).
24. Lu, H., Mack, J., Yang, Y. & Shen, Z. Structural modification strategies for the rational design of red/NIR region BODIPYs. *Chem. Soc. Rev.* **43**, 4778–4823 (2014).
25. Ni, Y. & Wu, J. Far-red and near infrared BODIPY dyes: synthesis and applications for fluorescent pH probes and bio-imaging. *Org. Biomol. Chem.* **12**, 3774–3791 (2014).
26. Wang, J., Boens, N., Jiao, L. & Hao, E. Aromatic [b]-fused BODIPY dyes as promising near-infrared dyes. *Org. Biomol. Chem.* **18**, 4135–4156 (2020).
27. Shukla, V. K., Chakraborty, G., Ray, A. K. & Nagaiyan, S. Red and NIR emitting ring-fused BODIPY/aza-BODIPY dyes. *Dyes Pigm.* **215**, 111245–111305 (2023).
28. Li, K. et al. J-aggregates of meso-[2.2]paracyclophanyl-BODIPY dye for NIR-II imaging. *Nat. Commun.* **12**, 2376 (2021).
29. Liu, Q. et al. Near-infrared-ii nanoparticles for cancer imaging of immune checkpoint programmed death-ligand 1 and photodynamic/immune therapy. *ACS Nano* **15**, 515–525 (2021).
30. Wang, X. et al. Discovery of BODIPY J-aggregates with absorption maxima beyond 1200 nm for biophotonics. *Sci. Adv.* **8**, eadd5660 (2022).
31. Zhu, Y. et al. Electron-withdrawing substituents allow boosted NIR-II fluorescence in J-type aggregates for bioimaging and information encryption. *Angew. Chem. Int. Ed.* **62**, e202313166 (2023).
32. Zu, B., Guo, Y. & He, C. Catalytic enantioselective construction of chiroptical boron-stereogenic compounds. *J. Am. Chem. Soc.* **143**, 16302–16310 (2021).
33. Zu, B., Guo, Y., Ren, L.-Q., Li, Y. & He, C. Catalytic enantioselective synthesis of boron-stereogenic BODIPYs. *Nat. Synth.* **2**, 564–571 (2023).
34. Guo, Y., Zu, B., Chen, C. D. & He, C. Boron-stereogenic compounds: Synthetic developments and opportunities. *Chin. J. Chem.* **42**, 2401–2411 (2024).
35. Ren, L.-Q. et al. Modular enantioselective assembly of multi-substituted boron-stereogenic BODIPYs. *Nat. Chem.* **17**, 83–91 (2025).
36. Zhan, B., Ren, L.-Q., Zhao, J., Zhang, H. & He, C. Catalytic asymmetric C–N cross-coupling towards boron-stereogenic 3-amino-BODIPYs. *Nat. Commun.* **16**, 438 (2025).
37. Braun, M. Boron-based enantiomerism. *Eur. J. Org. Chem.* **27**, e202400052 (2024).
38. António, J. P. M., Roque, I. L., Santos, F. M. F. & Gois, P. M. P. Designing functional and responsive molecules with boronic acids. *Acc. Chem. Res.* **58**, 673–687 (2025).
39. Abdou-Mohamed, A. et al. Stereoselective formation of boron-stereogenic organoboron derivatives. *Chem. Soc. Rev.* **52**, 4381–4391 (2023).
40. Li, X., Zhang, G. & Song, Q. Recent advances in the construction of tetracoordinate boron compounds. *Chem. Commun.* **59**, 3812–3820 (2023).
41. Lu, H., Mack, J., Nyokong, T., Kobayashi, N. & Shen, Z. Optically active BODIPYs. *Coord. Chem. Rev.* **318**, 1–15 (2016).
42. Gao, Y. et al. Catalytic enantioselective synthesis of boron-stereogenic and axially chiral BODIPYs via rhodium(II)-catalyzed C–H (hetero) arylation with diazonaphthoquinones and diazoindenines. *Angew. Chem. Int. Ed.* **64**, e202418888 (2025).
43. Mei, J., Leung, N. L. C., Kwok, R. T. K., Lam, J. W. Y. & Tang, B. Z. Aggregation-induced emission: Together we shine, united we soar!. *Chem. Rev.* **115**, 11718–11940 (2015).
44. Zhang, R. et al. Blood circulation assessment by steadily fluorescent near-infrared-II aggregation-induced emission nano contrast agents. *ACS Nano* **17**, 19265–19274 (2023).
45. Flock, S. T., Jacques, S. L., Wilson, B. C., Star, W. M. & van Gemert, M. J. Optical properties of intralipid: A phantom medium for light propagation studies. *Laser Surg. Med.* **12**, 510–519 (1992).
46. Li, B. et al. Organic NIR-II molecule with long blood half-life for in vivo dynamic vascular imaging. *Nat. Commun.* **11**, 3102 (2020).
47. Xu, J. et al. Biomimetic NIR-II fluorescent proteins created from chemogenic protein-seeking dyes for multicolor deep-tissue bioimaging. *Nat. Commun.* **15**, 2845 (2024).

Acknowledgements

We are grateful for financial support from the National Natural Science Foundation of China (22271134, 8237218), Guangdong Provincial Key Laboratory of Catalysis (No. 2020B121201002), Shenzhen Science and Technology Innovation Commission (RCJC20221008092723013, RCYX20221008092946108, JCYJ20230807093104009). The study was also supported by the Beatriu de Pinós program from AGAUR (Grant no. 2022 BP 00055 to Y.L).

Author contributions

C.H., J. Zhao and L.-Q.R. conceived the project. J. Zhao, L.-Q.R. and B.Z. designed and performed the synthetic experiments. J.M., D.L. and J. Zhang performed the bioimaging experiment. C.H., L.-Q.R., J.M. and J.Zhao prepared the manuscript. Correspondence should be sent to J.M. (jing.mu@pkuszh.com), C.H. (hec@sustech.edu.cn).

Competing interests

The authors declare no competing interests.

Additional information

Supplementary information The online version contains supplementary material available at https://doi.org/10.1038/s41467-025-64709-z.

Correspondence and requests for materials should be addressed to Jing Mu or Chuan He.

Peer review information *Nature Communications* thanks Zhipeng Liu, Hu Xiong, and the other, anonymous, reviewer for their contribution to the peer review of this work. A peer review file is available.